ZAGADNIENIA
EKSPLOATACJI
MASZYN
Zeszyt 1 (149) 2007

JAN BURCAN*, RADOSŁAW BEDNAREK*

Determination of the magnetic field distribution for high-energy magnets

Key words

High-energy permanent magnet, magnetic induction, magnetic field distribution.

Słowa kluczowe

Wysokoenergetyczny magnes trwały, indukcja magnetyczna, rozkład pola magnetycznego

Summary

The study presents the results of magnetic induction measurements in the vicinity of front ends of high-energy magnets. The character of the induction vector value changes as the function of the distance from the magnet front end, and as the function of the magnet diameter and its relative length, is presented. It has been proved that the distribution of the induction vector, beside the mentioned above values, is also influenced by shape and mounting errors of magnets, especially by the front end axial run-out and by the side surface radial run-out of the magnet, which result therefrom.

The knowledge of the course of the induction vector variations as a function of geometry and material parameters enables to determine precisely the variation of the repulsion force value of the co-operating magnets, thus will be helpful when designing pairs unloaded by means of the magnetic field, e.g. bearings or slides.

1. Introduction

Modern magnetic materials owe their usable parameters to the intrinsic magnetic properties of the intermetallic phases that constitute their composition, to the optimised microstructure, and to the chemical composition [1].

* Politechnika Łódzka, Katedra Konstrukcji Precyzyjnych, ul. B. Stefanowskiego 1/15, 90-924 Łódź, tel. (042) 6312249, e-mail: janbur@p.lodz.pl.

The present development of magnetic material goes towards improvement of the microstructure. New materials, called nanocrystal magnets, have appeared. Single-phase or double-phase magnets that consist of hard magnetic material in soft base material are distinguished. Their advantage is, besides good magnetic properties, high resistance to corrosion.

The occurrence of new materials was possible thanks to new methods of powder production and their consolidation – among others the magnetic materials as well, e.g. by explosion pressing or binding by means of polymer materials that enable to form unrestricted shapes of magnets.

The most often utilized hard magnetic materials, at present, are the rare earth metal sinters such as: Sm_2Co_{17} or $Nd_2Fe_{14}B$ with the rare earth metals Sm and Nd, respectively. A characteristic feature of the former is the resistance to high temperatures and demagnetizing fields, whereas that of the latter is higher remanence and lower price.

The team of the Department of Precise Constructions has been engaged in research works related to the load transfer by means of magnetic field since the 70ies of the last century [2]. At the beginning we designed and constructed aided systems, such as: the bearing system of the gramophone arm aided with magnetic field. In the next years we developed the construction and performed tests with longitudinal and radial bearings, passive and active as well. The have shown that the interaction force between two magnets is directly proportional to the product of their magnetic induction [3]. Therefore a precise data concerning distribution of magnetic induction is required in order to determine the forces induced by the magnetic field. If the distribution of the magnetic field is known the force vector may be defined precisely.

Referring to passive longitudinal bearings our investigations have shown a considerable influence of the front end shape of the co-operating magnets on the load capacity, stiffness, damping coefficient and other parameters of the bearings.

In order to determine exactly and to perform the analysis of the distribution of magnetic induction vector of high-energy cylindrical magnets a technically advanced testing device was developed that enabled to scan precisely the magnetic field in the space over the magnet surface [4].

2. Measurement method

2.1. Testing stand

The testing stand for determination of distribution of the magnetic induction vector [4] consists of the measuring head positioning assembly (1), the tested magnet positioning assembly (2), the measuring head (3), and the control and data collection system (4) (Fig. 1).

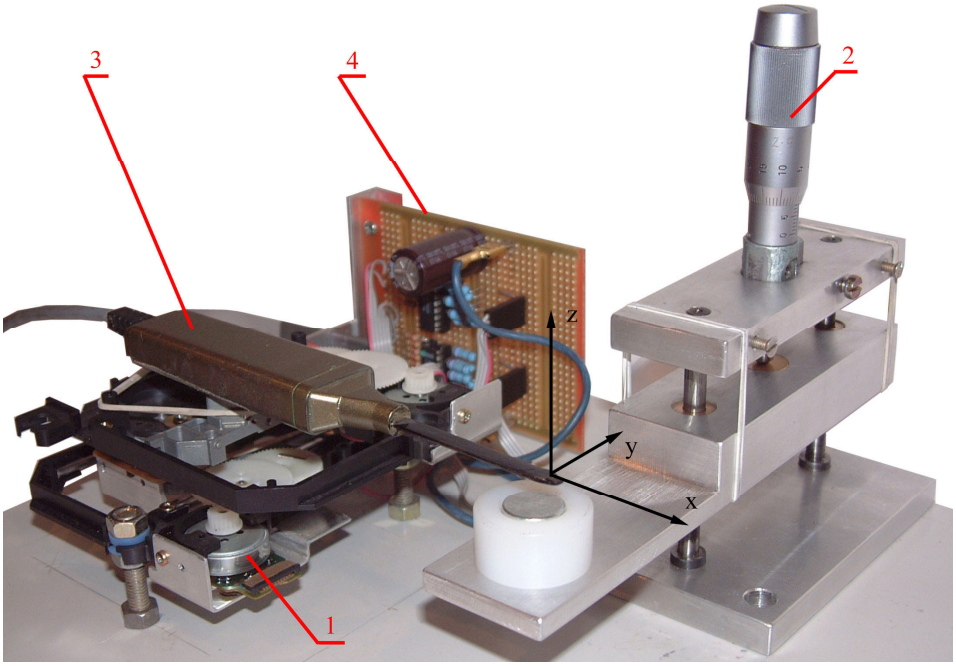

Fig. 1. Construction of the test stand
Rys. 1. Stanowisko pomiarowe

Data collection range in the 3D space of the dimensions 35x35x25 mm with the positioning accuracy 0,02 mm. The measuring head is provided with two inductive sensors based on the Hall effect (BH-200 manufactured by F.W. Bell), which are placed on planes perpendicular one to the other. This enables to measure simultaneously two components of the induction vector. The measuring range of the sensors is ±1 T. The sensor calibration error did not exceed 1,5% of the real value and it did not change for all measured specimens. The linearity error within the measured range did not exceed 0,5% of the indicated value.

Prior to measurements the angular location of sensors in relation to main axis of the system was checked. The angular deflection of the three sensor axes in relation to the main axis of the device did not exceed 1°. Out-of-parallel error of the sensor 1 which is responsible for the measurement of the vertical component of the induction, in relation to the horizontal plane, did not exceed 10'.

During first tests the effect of temperature on the error of measurement of magnetic induction was also determined. For the sensor 1 it was equal to $\varepsilon_{B1} = (0{,}00057 \cdot T - 0{,}01144)$ and for the sensor 2 $\varepsilon_{B2} = (0{,}00059 \cdot T - 0{,}01180)$, where ε_B – induction relative error (in %) and T –ambient temperature (in °C). The error ε_B for all measurements did not exceed ±0,06% of the indication.

Specially developed software enables to control, collect and store the data. Prior to the measurement it is possible to set the measurement range (±62,5 mT, ±125 mT, ±250 mT, ±500 mT or ±1 000 mT), scanning range, step (min. 0,1 mm) and the time that is necessary to move the measuring head by one step. One step means the time that is necessary to stop the system, collect 10 measurements, to determine the mean value and the measurement error in the defined point of the space, as well as to record the information in the table. The preliminary tests showed that the optimum time, considering technical possibilities and lowest errors was equal to 60 ms. Change of the measuring range does not create additional errors.

2.2. Preparation of specimens

Two cylindrical magnets made of the Neodymium-Iron-Boron sinter (N38) were used for tests. The remanence, coercive force and $(BH)_{max}$ for that sinter are equal respectively: $B_r = 1{,}23 \pm 0{,}02$ T; ${}_bH_c \approx 900$ kA/m; $(BH)_{max} = 294 \pm 0{,}08$ kJ/m^3. Marking of the tested specimens and their overall dimensions are presented in Table 1.

Table 1. Overall dimensions of magnets with specimen marking
Tabela 1. Wymiary gabarytowe magnesów wraz z oznaczeniami próbek

Specimens	L	L_{rz}	D	D_{rz}	$\frac{L}{D}$	$\left(\frac{L}{D}\right)_{rz}$	Max radial run-out.	Angle at which maximum radial run-out occurs	Max axial run-out	Angle at which maximum axial run-out occurs	Magnet front end declination angle
	mm	mm	mm	mm	–	–	mm	degrees	mm	degrees	degrees
2A	2	1,95	10	9,93	0,200	0,196	0,06	270	0,06	140	0,34
2C		1,95		9,94		0,196	0,09	240	0,03	10	0,17
2D		1,95		9,93		0,196	0,08	220	0,07	220	0,40
2E		1,96		9,93		0,197	0,21	290	0,09	50	0,52
3A	3	2,95	10	9,92	0,300	0,297	0,08	240	0,02	120	0,11
3B		2,94		9,93		0,296	0,07	320	<0,01	–	<0,06
3D		2,95		9,92		0,297	0,08	250	0,04	230	0,23
3E		2,92		9,93		0,294	0,11	320	0,05	260	0,29
4A	4	4,00	10	9,95	0,400	0,402	0,08	220	<0,01	–	<0,06
4B		3,99		9,96		0,401	0,06	250	0,03	270	0,17
4C		3,98		9,95		0,400	0,07	190	<0,01	–	<0,06
4E		3,98		9,95		0,400	0,11	180	0,05	280	0,29
5B	10	9,95	10	9,94	1,000	1,001	0,06	260	0,02	120	0,11
5C		9,97		9,93		1,004	0,04	260	0,03	260	0,17
5E		9,96		9,95		1,001	0,04	200	0,04	300	0,23
5F		9,95		9,96		0,999	0,08	210	0,08	120	0,46
8D	2	2,00	20	19,96	0,100	0,100	0,17	180	0,03	240	0,09
8E		2,00		19,95		0,100	0,03	240	0,04	150	0,11
8F		2,00		19,94		0,100	0,11	220	0,06	280	0,17
8G		1,99		19,96		0,100	0,05	240	0,02	270	0,06

Table 1 continued
Tabela 1 cd.

Speci-mens	L	L_{rz}	D	D_{rz}	$\frac{L}{D}$	$\left(\frac{L}{D}\right)_{rz}$	Max radial run-out	Angle at which maximum radial run-out occurs	Max axial run-out	Angle at which maximum axial run-out occurs	Magnet front end declination angle
	mm	mm	mm	mm	–	–	mm	degrees	mm	degrees	degrees
9A	2,5	2,49	20	19,90	0,125	0,125	0,05	90	0,05	220	0,14
9B		2,46		19,95		0,123	0,02	50	0,02	90	0,06
9C		2,50		19,95		0,125	0,08	230	0,08	310	0,23
9D		2,50		19,95		0,125	<0,01	–	0,02	350	0,06
10A	5	5,01	20	20,00	0,250	0,251	0,12	240	<0,01	–	<0,03
10B		5,01		20,00		0,251	0,08	250	0,03	280	0,09
10C		4,98		19,97		0,249	0,13	240	0,04	290	0,11
10D		4,99		20,01		0,249	0,13	220	<0,01	–	<0,03
11A	6	5,98	20	19,99	0,300	0,299	0,06	240	0,04	160	0,11
11B		6,00		19,97		0,300	0,02	140	0,06	240	0,17
11C		5,99		19,96		0,300	0,09	250	0,07	190	0,20
11D		6,00		19,98		0,300	0,11	230	0,03	330	0,09
6C	6	5,97	22	21,95	0,273	0,272	0,07	180	<0,01	-	<0,03
7D	10	10,03	22	21,99	0,455	0,456	0,12	300	0,10	190	0,26

Prior to the test the diameter D_{rz} and the length L_{rz} of each specimen was determined, that enabled to determine their surface area and volume. The magnets were pressed into adequately prepared plastic sleeves. Prior to the measurement the overall dimensions of the sleeves were measured. Axial and radial run-out of the sleeve surface that after the assembly contact the magnet, were also determined. Having installed the magnet the resulting axial play of the magnet front end related to the base was defined (Fig. 2). All measurements were performed with the accuracy 0,01 mm.

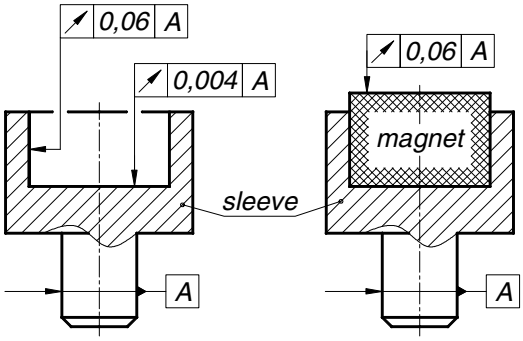

Fig. 2. Diagram of the test specimen with marked axial and radial measurement bases
Rys. 2. Schematyczny widok próbki pomiarowej z oznaczonymi bazami pomiarowymi bicia osiowego i promieniowego

2.3. Magnetic induction measurement

The magnetic induction measurements of all specimens are presented in Table 1. The measurements were performed over the monitored surface of the magnet at distances that changed in steps within the range from $z = 0$ to 5 mm, every 0,1 mm. The measurements were performed for different angular positions of the specimen (every 30°) as a function of the magnet radius R (Fig. 3). The measurements were performed at temperature $T = 20\pm1°$, and relative humidity 58±7%.

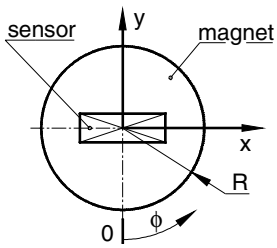

Fig. 3. Adopted polar coordinate system against a background of Cartesian coordinate system together with view of the sensor over the surface of the magnet (dia10 mm)

Rys. 3. Przyjęty układ współrzędnych biegunowych na tle współrzędnych kartezjańskich wraz z obrazem czujnika naniesionym nad powierzchnią magnesu o średnicy 10 mm

An example of testing results for the specimen 2A are given in Figs. 4 and 5.

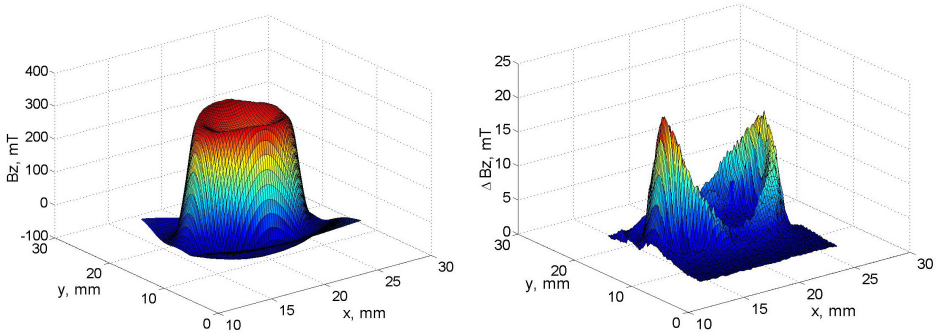

a) b)

Fig. 4. Example of testing results for the specimen 2A, presented in Cartesian coordinate system (x-y) for the minimum distance from the magnet end face resulting from maximum axial run-out ($z < 0{,}06$ mm): a) changes of vertical components (axis z) of the magnetic induction vector, b) registered measurement error

Rys. 4. Przykładowe wyniki pomiaru uzyskane dla próbki 2A, przedstawione w układzie kartezjańskim (x-y), dla minimalnej odległości od czoła magnesu, wynikającej z max bicia osiowego ($z < 0{,}06$ mm): a) przebieg składowych pionowych (w osi z) wektora indukcji magnetycznej, b) zarejestrowany błąd pomiaru

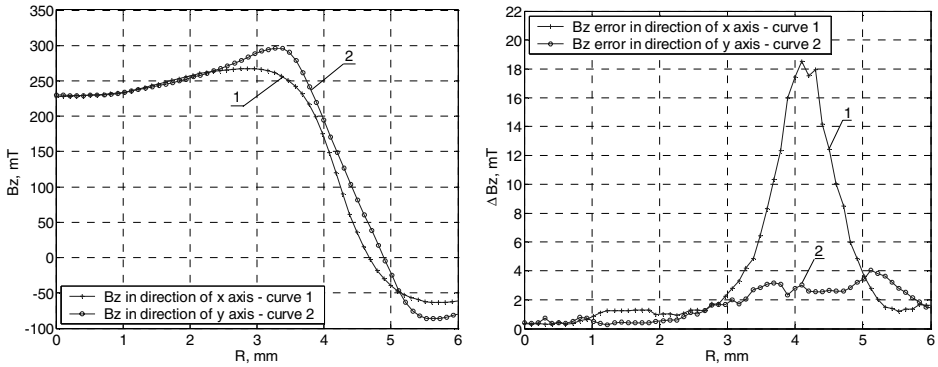

a) b)

Fig. 5. Example of testing results for the specimen 2A, presented in polar coordinate system (R, ϕ (for ϕ = 0º)), measurements along x and y for minimum distance from the magnet face, resulting from maximum axial run-out (z < 0,06 mm): a) changes of vertical components (axis z) of the magnetic induction vector, b) registered measurement error

Rys. 5. Przykładowe wyniki pomiaru uzyskane dla próbki 2A, przedstawione w układzie biegunowym (R, ϕ (dla ϕ = 0º)), pomiary w kierunku osi x i y dla minimalnej odległości od czoła magnesu, wynikającej z max bicia osiowego (z < 0,06 mm): a) przebiegi składowych pionowych (w osi z) wektora indukcji magnetycznej, b) zarejestrowany błąd pomiaru

As can be noticed in the Fig. 5, the absolute error values along the x axis compared to the error values along the y axis are much bigger respectively in planes y-z and x-z that pass through the vertical symmetry axis of the magnet. This dependence was repeated for all discussed specimens so it can be related to the sensor shape (Fig. 3). Therefore, the changes of induction in the plane y-z are considered further.

Figure 6 shows an example of results obtained for the specimen 2A for various angular positions in the plane x-y. It should be noted that the maximum value of the

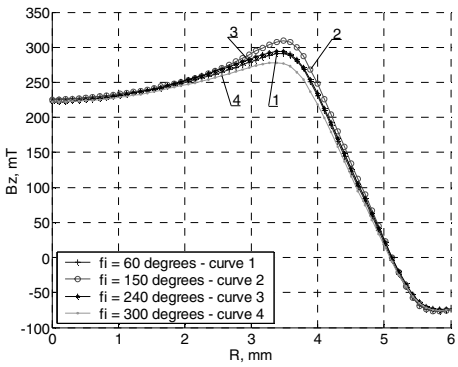

Fig. 6. Example of changes of the magnetic induction vector components for the specimen 2A for the minimum distance from the magnet face as the function of the specimen radius R for various angular positions: ϕ = 60º (Bz = 291 mT); 150º (Bz = 309 mT); 240º (Bz = 293 mT) and 330º Bz = 280 mT)

Rys. 6. Przykładowe przebiegi składowych wektora indukcji magnetycznej dla próbki 2A, dla minimalnej odległości od czoła magnesu, w funkcji promienia próbki R, dla różnych położeń kątowych ϕ = 60º (Bz = 291mT), 150º (Bz = 309mT), 240º (Bz = 293mT) i 330º (Bz = 280 mT)

induction vertical component occurs at the angle 150º, which is located near the angle where the maximum axial run-out of the edge occurs (Table 1).

2.4. Test results

The obtained test results enabled to perform initial analysis of the variations of the value of the vertical component of the induction vector, for different distances from the magnet face (Figs. 7 and 8).

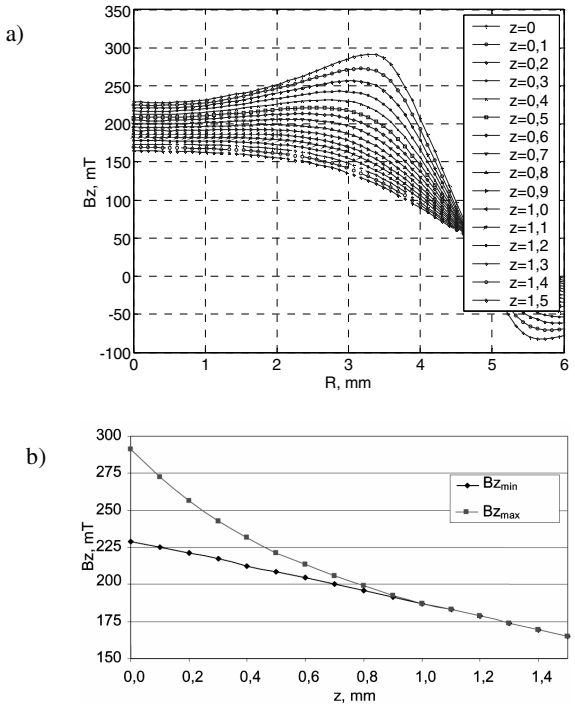

Fig. 7. Variation of the value of vertical component of magnetic induction as a function of distance z from the magnet face for the specimen 2A: a) Bz as a function of z and R for $\phi = 0º$, b) Bz_{min} as a function of z for $R = 0$ and $\phi = 0º$, and Bz_{max} as a function of z for R_{max} and $\phi = 0º$, where R_{max} is the radius for which the vertical component of the induction reaches its maximum value Bz_{max}
Rys. 7. Zmiana wartości składowej pionowej indukcji magnetycznej w funkcji odległości od czoła magnesu, z, dla próbki 2A: a) Bz w funkcji z i R, dla $\phi = 0º$, b) Bz_{min} w funkcji z, dla $R = 0$ i $\phi = 0º$, oraz Bz_{max} w funkcji z, dla R_{max} i $\phi = 0º$, gdzie R_{max} – promień, na którym znajduje się wartość maksymalna pionowej składowej indukcji Bz_{max}

An example of the results obtained for the specimen 2A are given in Fig. 7: the course of the variations of Bz value as a function of distance z from the magnet face and radius R for $\phi = 0º$ (Fig. 7a) and the course of the value Bz_{min} (for $R = 0$) and Bz_{max} (for $R = R_{max}$) as a function of distance z from the magnet face for $\phi = 0º$ (Fig. 7b). R_{max} is the distance from the axis, for which the value of the vertical component of the induction is maximum. R_{max} decreases and approaches to zero if the distance from the magnet face increases.

The course of the variations of *Bz* value as a function of distance *z* from the magnet face, for $R = 0$ and $\phi = 0°$ for selected specimens from Table 1 are given in Fig. 8.

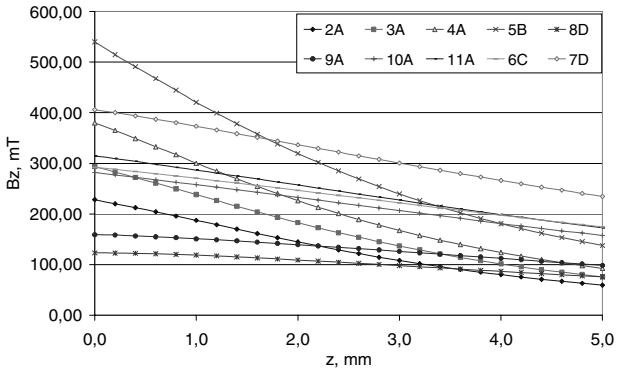

Fig. 8. Variation of the value of the vertical component of magnetic induction as a function of *z* for $R = 0$ and $\phi = 0$, for selected specimens from Table 1

Rys. 8. Zmiana wartości składowej pionowej indukcji magnetycznej w funkcji z, dla R = 0 i ϕ = 0, dla wybranych próbek z tabeli 1

Example of the results are presented in Fig. 9.

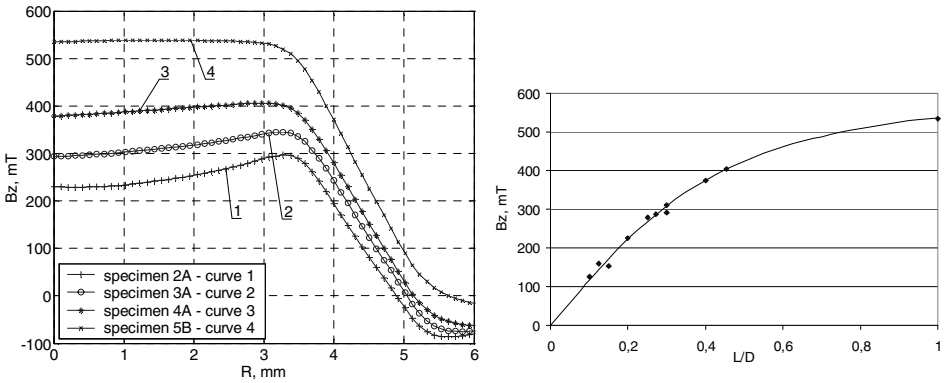

a) b)

Fig. 9. Influence of the magnet height on the values and variations of the vertical component of magnetic induction at the minimum distance from the magnet face for various magnets (maximum axial run-out – see Table 1): as a function of *R* for $\phi = 0$ and $z = 0$ for the specimens: 2A, 3A, 4A and 5B, as a function of *L/D* for $R = 0$, $\phi = 0$ and $z = 0$ for the specimens:1E, 2A, 3A, 4A, 5B, 8D, 9A, 10A, 11A, 6C and 7D (dimensions are given in Table 1)

Rys. 9. Wpływ wysokości magnesu na wartość i przebiegi pionowej składowej indukcji magnetycznej, w minimalnej odległości od czoła magnesu (max bicie osiowe – tabela 1), dla różnych magnesów: w funkcji R, dla ϕ = 0 i z = 0 – próbki: 2A, 3A, 4A i 5B, w funkcji (L/D), dla R = 0, ϕ = 0 i z = 0 – próbki:1E, 2A, 3A, 4A, 5B, 8D, 9A, 10A, 11A, 6C i 7D (wymiary w tabeli 1)

On the base of the results of the tests it can be affirmed that the values of the vertical component of magnetic induction are influenced by: the length L and diameter D of the magnet and, moreover, by the relative height of the magnet L/D. With a good approximation the values of the vertical component of magnetic induction for $R = 0$ and $z = 1$ are described by the relation 1:

$$Bz = \frac{B_r}{2}\left(\frac{\frac{L}{D}}{\sqrt{\frac{1}{4}+\left(\frac{L}{D}\right)^2}}\right) \tag{1}$$

where: B_r denotes remanence (in T).

3. Conclusions

On the basis of the analysis of the test results an important influence of the sensor size on the variations of vertical component of magnetic induction can be noticed. In Fig. 5 the distance Bz_{max} from the magnet axis for the measurement in x direction is smaller than the one achieved in y direction. This result is closely related to the magnet length in the direction of the measurement and to the magnet curvature as well as to the width of the sensor in the direction perpendicular to the direction of the measurement (Fig. 3). It follows from that Bz_{max} is reached for a point in which the whole surface of the sensor is placed over the magnet surface. It can be concluded that the sensor averages out the values of induction from its whole surface. Therefore the ratio of the length to the diameter of the magnet as well as the ratio of the surface of the sensor to the face area of the measured magnet are essential.

The error of fixing the magnets in sleeves has a crucial influence on the distribution of the magnetic induction, especially on the axial run-out of the magnet face and on the radial run-out of the magnet side surface that result thereof. Due to the axial run-out of the end face of the magnet gaps with various values are created. The radial run-out of the side surface of the magnet determines the shift of the magnet axis in relation to the axis of the measurement assembly.

The distance from the magnet surface influences to a great extent the value of the vertical component of magnetic induction. Bearing in mind that the repulsion force between two magnets is proportional to the product of the induction value of each one we can expect in case of magnets the faces of which are not parallel to each other that the moment of force will occur which will create the tendency to turn the magnets or will create a tangential force that will push out the magnets in the radial direction.

For the system consisting of two magnets interacting each other with a force of repulsion the most important parameters for stability of the system are parallelism and coaxiality of surfaces of their working faces.

The ratio Bz_{max}/Bz_{min} decreases for increasing values of the ratio *L/D*, and achieves the value near to one for *L/D* = 1 (Fig. 9a). It follows from that the distribution of the vector of induction over the magnet surface as a function of *R* for increasing values *L/D* ratio tends to a horizontal line that does not depend on the value of the radius (curve 4 in Fig. 9a).

It is more easy to assemble magnets with greater value of the *L/D* ratio. Simultaneously, for magnets with greater values of *L/D* a smaller influence of the axial run-out on the value of magnetic induction may be perceived. For instance, the relative error of the induction, i.e. the difference of induction values for following angular positions of the specimen 2A (with *L/D* = 0,2), in relation to the maximum value of the induction, for the maximum axial run-out equal to 0,06 mm overcame 9% (Fig. 6). For the specimen 5F, for which the ratio *L/D* was equal to 1, the maximum axial run-out was equal to 0,08 mm and the relative induction error did not overcome 2%.

When the value of the parameter *L/D* increases, the value of the vertical component of magnetic induction increases as well and reaches probably a value approximately equal to half of the value of the magnetic remanence of the material (Fig. 9b). As an example, for *L/D* = 0,5 the ratio of the value of vertical component and remanence is equal approximately 71%, for *L/D* = 1 approximately 90%, and for *L/D* = 2 approximately 97%. As can be easily noted the increase of the value of the induction is smaller when the value of the parameter *L/D* increases. Simultaneously, together with the increase of the *L/D* ratio the volume of the magnet increases. *An increase of the price of the magnet proportional to the increase of the L/D parameter may substantially influence the selection of a magnet during designing.* Therefore the value of the vertical component of magnetic induction depends on the value of the *L/D* parameter, but there exists its optimum value, for which the minimum volume of a magnet is achieved when appropriate value of the induction is maintained.

An increase of the magnet diameter at constant *L/D* ratio influences the gradient of the $Bz = f(z)$ curves (Fig. 8). For greater diameters the gradient of the Bz value is much lower, and the curve tends to a straight line with the slope considerably smaller. Changing the parameter *L/D* the value of the horizontal component of magnetic induction may be easily adjusted.

The force of repulsion between two magnets facing each other, is proportional not only to the induction value of the magnets but also to the areas of their working surfaces. At a constant value of the magnetic induction and at constant *L/D* ratio different values of repulsion forces are created for different magnet diameters. On the other hand different forces can be created for the same value of the diameter when the *L/D* ratio will change. In the first case the change of the force depends on the change of the working area of the magnets and in the

second one it depends on the induction value. Due to lower gradient of the induction value as a function of the distance from the face of the magnet the first case seems to be more favourable in systems where the distance between magnets may change, for instance, due to vibrations.

List of symbols:

B_r – remanence [T],
Bz – vertical component of magnetic induction of the magnet [T],
Bz_{max} – maximum value of the vertical component of magnetic induction for $R = R_{max}$ [T],
Bz_{min} – minimum value of the vertical component of magnetic induction for R = 0 [T],
D – magnet diameter [mm],
D_{rz} – real value of magnet diameter (from the measurement) [mm],
L – magnet height [mm],
L_{rz} – real value of magnet height (from the measurement) [mm],
(L/D) – relative height of the magnet,
$(L/D)_{rz}$ – relative height of the magnet for L_{rz} and D_{rz},
R – magnet radius [mm],
R_{max} – magnet radius for which Bz_{max} occurs [mm],
T – ambient temperature during measurements [ºC],
Z – distance of the measured surface from the front face of the magnet [mm],
ΔBz – absolute error of the measurement of the vertical component of magnetic induction [T],
ε_B – relative error of the sensor indication depending on the ambient temperature during the measurement [%].

Praca wpłynęła do Redkacji 02.02.2007 r.

References

[1] Leonowicz M., Wysłocki J.J., Modern magnets *[Współczesne magnesy]*. WNT, Warszawa 2005.
[2] Burcan J., Magnetic field aided bearings *[Łożyska wspomagane polem magnetycznym]*. WNT, Warszawa1996.
[3] Sławińska A., Examination of static and dynamic characteristics of longitudinal magnetic passive bearings in the aspect of design and material features *[Badanie charakterystyk statycznych i dynamicznych wzdłużnych magnetycznych łożysk pasywnych w aspekcie cech konstrukcyjnych i materiałowych]* Ph.D. Thesis under direction of prof. J. Burcan, Technical University of Łódź [Rozprawa Doktorska pod kierunkiem prof. J. Burcana, Politechnika Łódzka, Łódź] 2004.

[4] Burcan J., Bednarek R., Change of the magnetic induction vector for various shapes of working surfaces of the magnet front ends *[Zmiana wektora indukcji magnetycznej dla różnych kształtów powierzchni roboczej czół magnesów]*. VIIth Problems of Unconventional Bearing Systems, Łódź, pages 79-82 [VII Problemy Niekonwencjonalnych Układów Łożyskowych, Łódź, s. 79-82] 2005.

Wyznaczanie rozkładu pola magnetycznego dla magnesów wysokoenergetycznych

S t r e s z c z e n i e

W pracy przedstawiono wyniki pomiarów indukcji magnetycznej w otoczeniu czół wysokoenergetycznych magnesów. Przedstawiono charakter zmian wartości wektora indukcji w funkcji odległości od czoła magnesu oraz w funkcji średnicy magnesu i względnej jego długości. Wykazano, iż na rozkład wektora indukcji, oprócz wymienionych wielkości, mają również wpływ błędy kształtu i osadzenia magnesów, szczególnie wynikające z nich bicie osiowe czoła i bicie promieniowe powierzchni bocznej magnesu.

Znajomość przebiegu zmienności wektora indukcji w funkcji parametrów geometrycznych i materiałowych umożliwia dokładne określenie zmienności wartości siły odpychania współpracujących ze sobą magnesów, co z kolei będzie pomocne przy projektowaniu węzłów odciążanych polem magnetycznym, na przykład łożysk czy prowadnic.